D R A F T 3 November 2017

The Quadrupole RF System: Design and Simulations

On Kim[1,2], Seungpyo Chang[1,2], Juhoon Choi[1,2], Selcuk Haciomeroglu[2], Soohyung Lee[2], B. Lee Roberts (editor)[3], David Rubin[4] Yannis K. Semertzidis[1,2]
[1]Korea Advanced Institute of Science and Technology
[2]Instituted of Basic Science / Center for Axion and Precision Physics
[3]Boston University
[4]Cornell University

I. INTRODUCTION

While the CERN and E821 scraping scheme of powering the electrostatic quadrupoles asymmetrically worked well for E821, the muon losses at late times were higher than desired for E989. The systematic error from muon losses in E821 was listed as 100 ppb, which was signifantly smaller than the dominant ones [1]. The coherent betatron oscillations (CBO) systematic error was listed as 70 ppb for the 2001 data set [1]. The goals for these errors stated in the E989 TDR are 20 ppb and < 30 ppb respectively. Another factor to remember is that the number of muons that were lost using this asymmetric scraping method was on the order of 15 to 20%, or perhaps even larger. The proposed RF system, which will scrape the beam and reduce the phase space, is calculated to lose around 5% of the beam, and to reduce or eliminate the systematic errors from both muon losses and the (CBO).

An RF voltage is applied to the quadrupole plates in the ring, rather than the asymmetric powereing of the quads has been proposed, which simulations show will significantly reduce both losses and the CBO. Already in 2003 it was suggested to add an RF dipole field to the ring to damp the CBO [2]. More recently it was realized that it would be possible to use an RF quadrupole field to cool the beam and reduce the losses. This system of simultaneously applying both types of RF fields has the potential to reduce both systematic errors significantly, to the projected levels in the TDR. The RF can be applied to all of the quads in the ring, or to a smaller number. The advantage applying it to all of the quadrupoles permits the RF voltage to be smaller to produce the same scraping effect.

Howard, who designed the quad pulsers, believes that the appliation of RF to the quads should be ok with the pulsers, as long as the capacitance of the system is not larger than that in the proposed design.

A. The proposed RF Scraping Scheme and Simulations

In the simulations the following conditions are assumed:

- A uniform magnetic field of 1.45 T
- The electrostatic quadrupoles go uniformly around the storage ring.
- The RF is applied to a single quadrupole. i.e. at one point in the ring located where a physical quadrupole is placed.
- The quadrupole and 20-pole components of the electrostatic quadrupole field is included in the simulation
- The distribution of 8,411 muons that come through the inflector and have been kicked by the kicker prototype pulse simulated by Seungcheon Kim [3] is used.

There are three ingredients in the simulation:

1. An RF quadrupole at the horizontal CBO frequency is applied to the quadrupole plates as shown in Fig. 1(a).
2. An RF dipole with the horizontal CBO frequency is applied to the same quad plates as shown in Fig. 1(b).

3. An RF quadrupole is also applied to the same plates with the vertical waist frequency as shown in Fig. 1(c).

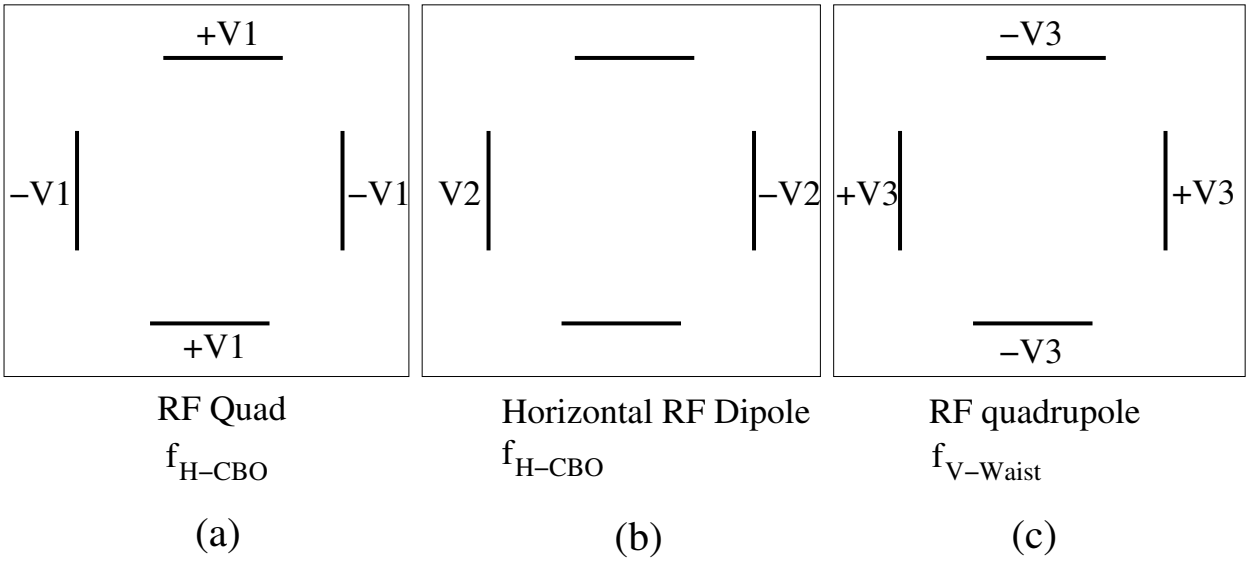

FIG. 1: The three contributions to the RF to be applied to the quadrupole plates. The sum of these three will be applied to a single plate. (a) The RF quadrupole field at $f_{\rm CBO}$. (b) The RF dipole field at $f_{\rm CBO}$. (c) The RF quadrupole at $f_{\rm VW}$

The RF quadrupole frequencies have the same voltage amplitude, although that could be changed to optimize the scraping. The horizontal RF dipole voltage has to be adjusted separately to optimize the elimination of the CBO.

The horizontal CBO frequency is 490 kHz, and the vertical waist frequency is 1.7 MHz. In principle one could use a vertical oscillating dipole field, but the vertical CBO frequency is 2.5 MHz, which is too high for the bandwidth of the RF amplifiers which specify the guaranteed bandwidth to be 10 kHz - 3 MHz.

The principle of the RF at the vertical waist frequency is shown in Fig. 2. During the application of the RF, the vertical phase space is modified so that the beam is scraped on the collimators, and then relaxed back to its equilibrium phase space. The amplitude and phase of each of these RF components can be adjusted to optimize the final beam. In principle the horizontal scraping could be done with the RF quadrupole as well, where Fig. 2 would have $x, x\prime$ rather than $y, y\prime$.

This same principle could also be used to scrape horizontally, where in Fig. 2 $x, x\prime$ is substituted for $y, y\prime$

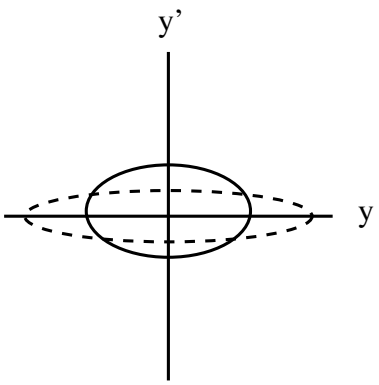

FIG. 2: The beam vertical phase space. The solid cuve shows the vertical acceptance of the ring, and the dashed ellipse shows the modification to the the RF quadrupole at the vertical waist frequency.

II. SIMULATIONS

A. KAIST Simulations

1. Introduction to KAIST Simulations

A homemade spin-tracking program has been used, written in `C++`. The lattice information is following.

- The ring has a radius 7.112 m.
- The collimator has a radius 45 mm, and is *continuous* along the ring circumference. Particles are *immediately* lost when they touch the collimator wall.
- A single detector is located at the fixed position.
- Neither inflector nor kicker is implemented.

The magnetic field is implemented homogeneous and uniform.

$$\mathbf{B} = B_0 \hat{y}, \tag{1}$$

where $\hat{y}$ points a direction perpendicular to the ring plane. B_0 is set to 1.451 T.

The electrostatic quadrupole is implemented to be *continuous* along the storage ring. Taking this account, the voltage is set to maintain the field index $n = 0.141$. The high voltage of the discrete quadrupoles of the realistic ring corresponding to this field index is 24 kV. The 20-pole correction to the quadrupole field is taken into account, adding 9th order term with respect to x and y into the linear field equation. The ratio between the 20-pole component and the quadrupole component of the electric potential used in the simulation is around 2%.

$$\mathbf{E} = E_0^{\text{4-pole}} \left(\frac{r}{r_0}\right) (\cos\theta, -\sin\theta, 0) + E_0^{\text{20-pole}} \left(\frac{r}{r_0}\right)^9 (\cos(9\theta), -\sin(9\theta), 0), \tag{2}$$

which is described in the accelerator coordinates again, where $r_0 = 45$ mm is the collimator radius and (r, θ) is the polar coordinates with respect to the (x, y) in the accelerator coordinates. The field strength at $(x, y) = (45$ mm, 0 mm) is given

$$E_0^{\text{4-pole}} = 0.38 \text{ MV/m}, \qquad E_0^{\text{20-pole}} = -0.038 \text{ MV/m}. \tag{3}$$

Those values were scaled with 156/360 to compensate the continuous quadrupoles from the discrete quadrupoles occupying 156° out of the ring circumference.

The RF electric field is applied to a localized region, in this case Q1S only, occupying 13° in azimuth. Basically we can come up with two different RF field, one is quadrupole field and the other is dipole field.

2. Simulations without and with RF

Figure 3 shows the beam horizontal mean(centroid) and RMS(width) as a function of time until 200 μs which approximately corresponds to 1341 turns for muons rotating around the design orbit. The amplitude of the mean oscillation, which also can be seen as the CBO amplitude, started around 10 mm and slowly being reduced with a lifetime $\sim$100 μs. The CBO amplitude is reducing because the 20-pole field shakes the Betatron oscillation frequency of the muons near the quadrupole plates.

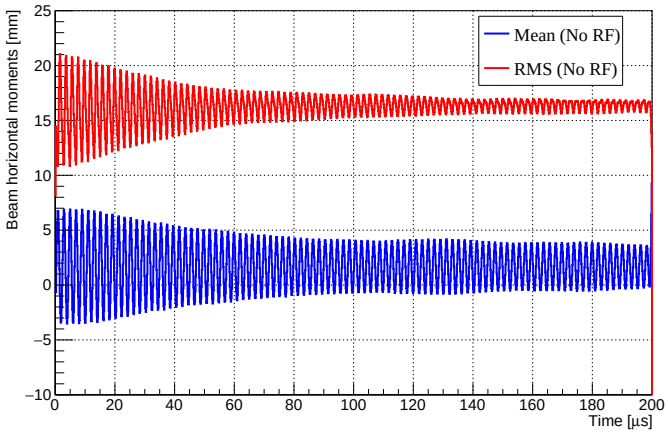

FIG. 3: Horizontal mean and RMS with no RF applied.

The reason why there's such a large oscillation for the first 100 μs can be explained by the fact that the high momentum muons and the low momentum muons are not lying on the exactly opposite phase in the horizontal phase space as shown in Figure 4. This is more clearly shown in Figure 5. The mean oscillation for the high momentum muons ($p > p_{\text{magic}}$) and the low momentum muons ($p < p_{\text{magic}}$) have a different phase to each other, not being cancelled as a total. This is dealt with by introducing the RF electric field oscillating with the CBO frequency as in Figure 6. Two different RF modes were applied, namely the dipole field and the quadrupole field. Both of them can resonate the beam and manipulate their phase space. With the dipole field oscillating with the CBO frequency, all muons are resonant with the field so it's capable of scraping the muon beam and also of modulating

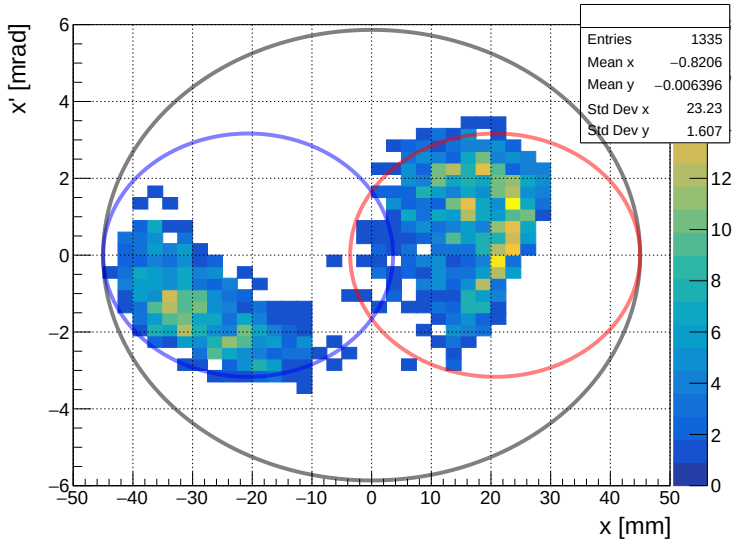

FIG. 4: Horizontal phase space only for the muons whose momentum difference with the magic momentum is higher than 0.2% ($|\mathrm{d}p/p| > 0.2\%$). The black, red and blue ellipses are the acceptance of the magic momentum muon, the high momentum muon (+0.25%) and the low momentum muon (−0.25%), respectively.

TABLE I: RF parameters.

Q1S RF	Dipole	Quadrupole
Amplitude [kV]	5	5
Freqeuncy [kHz]	520	490
Phase [deg]	0	90
Duration [μs]	0-5	5-15

the Betatron oscillation frequency. This can be seen by comparing the blue curve (with RF) and the green curve (without RF) or the red curve (with RF) and the yellow curve (without RF) in Figure 7. Indeed during the first 5 μs when the dipole field is being applied, the CBO frequencies of the high momentum muons and the low momentum muons were shifted. This dipole field was applied until their phase becomes exactly opposite to each other, and then the RF quadrupole field was applied for another 10 μs to reduce their amplitude altogether. Even thought there are several small growths and cool downs in CBO oscillation with RF in Figure 6, the all RF field was turned off at 15 μs, not to have a possibility of disturbing other electronic systems or the stable muon storage especially during the data taking period. Only 5% of muons were lost due to the RF field. In Figure 8, one can check the RF field reduced both the mean and RMS of the horizontal distribution. Those are horizontal phase spaces at 80 μs, where one is without RF and the other is with RF.

The RF parameters I have used in this simulation are in Table I. 5 kV amplitude of RF electric potential is not small, and in the real experiment we are restricted to apply under 1 kV to avoid undesirable sparks and interferences, also because of the hardware limitations. However, we can expect the same effect using the parameters in Table I with expanding the RF region.

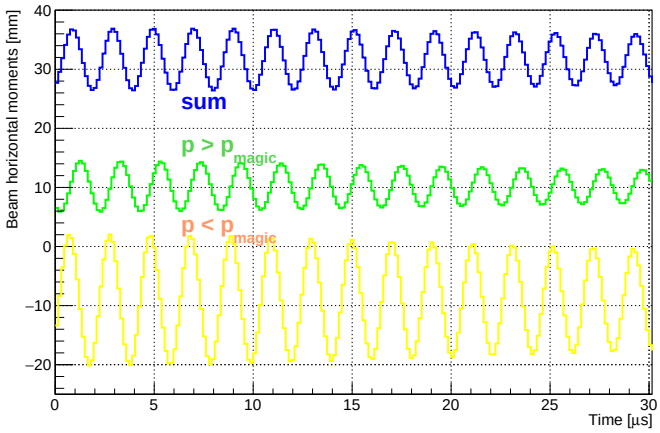

FIG. 5: Horizontal mean of the muons with upper magic momentum and those with lower magic momentum. The total mean is represented as "sum" and it has a 30 mm vertical offset in this plot.

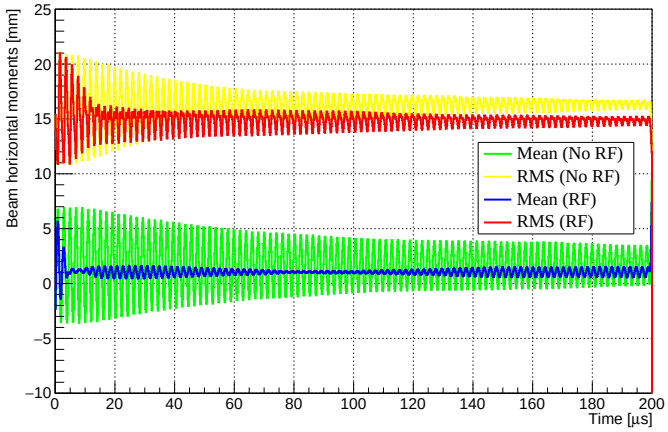

FIG. 6: Horizontal mean and RMS.

3. Summary of KAIST Simulations

In this simulation study, it is proved that the RF electric field oscillating with the CBO frequency can reduce the CBO amplitude significantly, without losing more than 5% of muons.

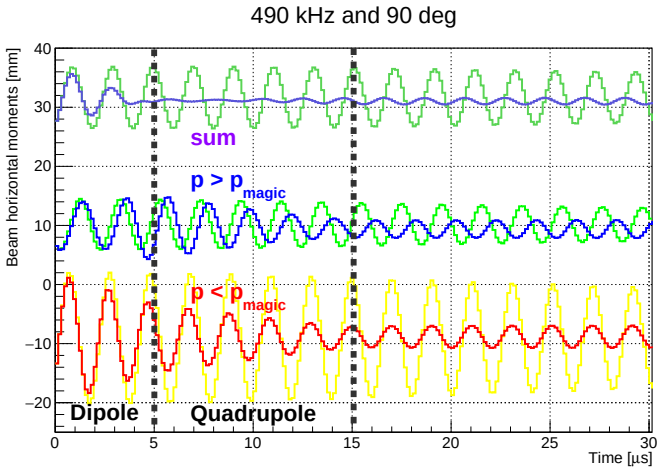

FIG. 7: Horizontal mean of the muons with upper magic momentum and those with lower magic momentum when the RF field is applied. The total mean is represented as "sum" and it has a 30 mm vertical offset in this plot. The blue, red and purple curves are the results with RF.

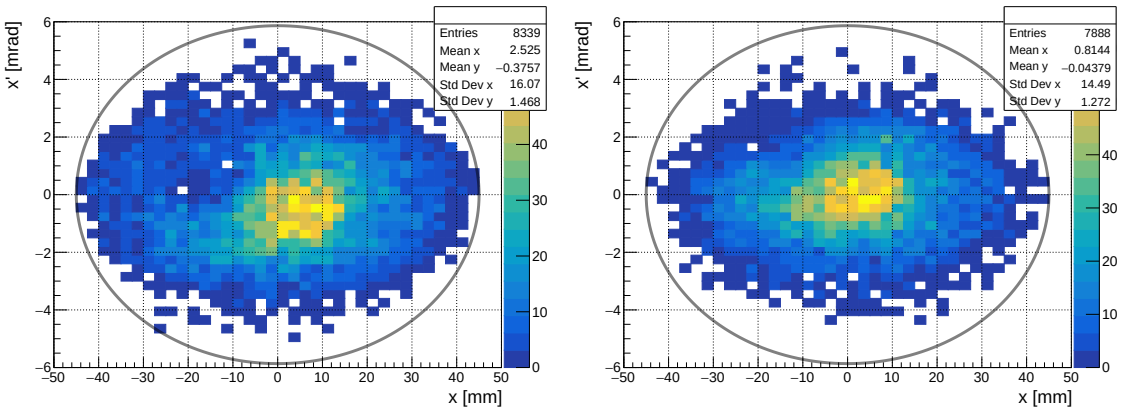

(a) (b)

FIG. 8: (a) The horizontal phase at 80 μs when there was no RF field, (b) when the RF field was applied with the parameters in Table I.

B. Cornell Simulations

That there is a mismatch of the beta-functions (β) and the dispersion (η) from injection channel into the storage ring is well know. The final focus quadrupoles in the M5 line are tuned so that there is a waist with $\beta_x \sim 1.5$m in the inflector. Dispersion in the inflector is zero. The closed ring twiss parameters are $\beta_x \sim 8$m and $\eta \sim 8.5$m. The effect of the mismatch is a β and η beat in the ring and modulation of beam width. The β-beat (quadrupole error) evolves at twice the CBO frequency and is thus can be mitigated by modulation of the quadrupole field at twice the CBO frequency with appropriate phase. The dispersion beat (dipole error) propagates at the CBO frequency and is compensated by modulating the quadrupole field at f_{CBO}, again with appropriate phase. The RF quad will evidently compensate dispersion and the beam width associated with the energy spread, or beta and the width from emittance, but not both. Best to demonstrate that we can reduce one without exacerbating the other. The RF quad of course effects vertical as well as horizontal and to the vertical betatron motion and dispersion. As there is no vertical bending in the ring, there is no way to compensate vertical dispersion (if there is any). If the RF frequency is not comensurate with vertical tune, (or multiples), then it will presumably have no significant effect on the vertical distribution.

Here we explore response of a momentum distribution to an RF quad voltage with horizontal CBO frequency in simulation. For all simulations the ring model includes quadrupoles and collimators. The RF voltage is applied to Q2 short.

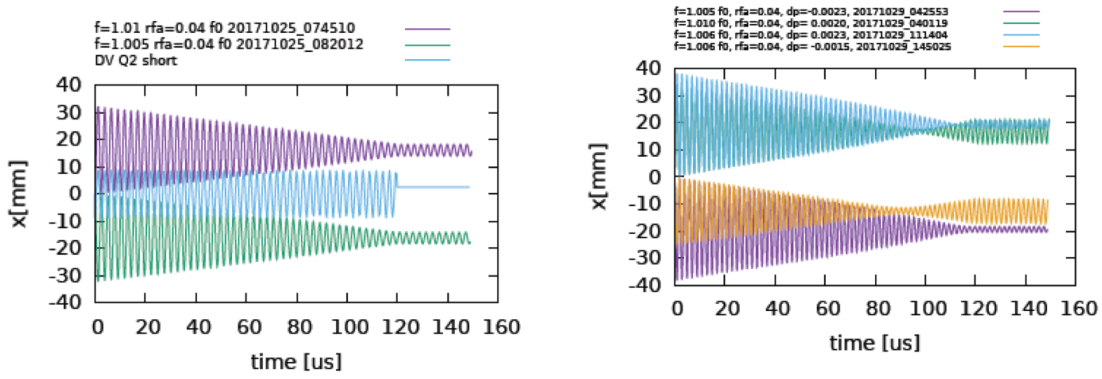

(a) (b)

FIG. 9: (a)A single particle with zero position offset, but $\pm 0.2\%$ momentum offset. Q2 short voltage modulated with f_{RF}. The CBO frequency depends on momentum. The effectiveness of voltage modulation depends on $f_{CBO} - f_{RF}$. (b)The most effective RF frequency depends on particle momentum. RF frequency for each trace is indicated in the key.

A complication is that the CBO frequency is momentum dependent, due both to the momentum dependence of the cyclotron frequency, and the chromaticity. In Figure 9(a) two particles with $\Delta p/p \pm 0.2\%$ momentum offset, but zero transverse offset or angle, are tracked for 150μs. The quadrupole voltage is shown as the middle trace. The frequency of the voltage modulation is chosen to match the CBO for that particular energy, determined by scanning frequency and finding the most effect at shrinking the oscillation, that is $f_{\pm} = (1 \pm 0.0025) f_0$, where f_0 is the CBO frequency for the on momentum muon. Note that as the amplitude

of the oscillation decreases, the trajectories converge to the closed orbits corresponding to the closed ring dispersion. Namely, at $x = \eta(\Delta p/p)$. Figure 9(b) includes other momenta and further illustrates the momentum dependence of the most effective quad frequency. The amplitude of the RF voltage here is about 1kV, and is turned off at 120μs.

In order to determine the RF frequency that will compensate dispersion for the anticipated distribution of momenta, we extend the excercise illustrated above to all momenta that are stored. For each of the momenta indicated in Figure 10(a) the frequency is tuned for most effectve damping. We see that within the region where the quad field is approximately linear, that the momentum dependence is linear as well. But for trajectories that are close to the quad plates the field gradient disappears. The field is nearly uniform. The CBO frequency and the corresponding best RF frequency change abruptly. Of course, insofar as the RF quad is meant to mitigate the lost muon systematic, it is these very far off momenta muons that are perhaps most important. We found that as long as the RF pulse is relatively short, it is indeed possible to mitigate the dispersion mismatch for muons of all momenta that are stored by suitable choice of RF frequency. In particular we find that a frequency of $f_{RF} = 0.985 f_0$ (see Figure **??**) is effective for all momenta.

While it is clear that the $f_{RF} \sim f_{CBO}$ mitigates momentum oscillations, it remains to demonstrate its effect on magic momentum muons with large betatron amplitude. And that we attempt to show in Figure 10(b) where we plot the trajectory of the magic momentum muon with amplitude 23mm and see that it is indeed unaffected by the RF on Q2 short.

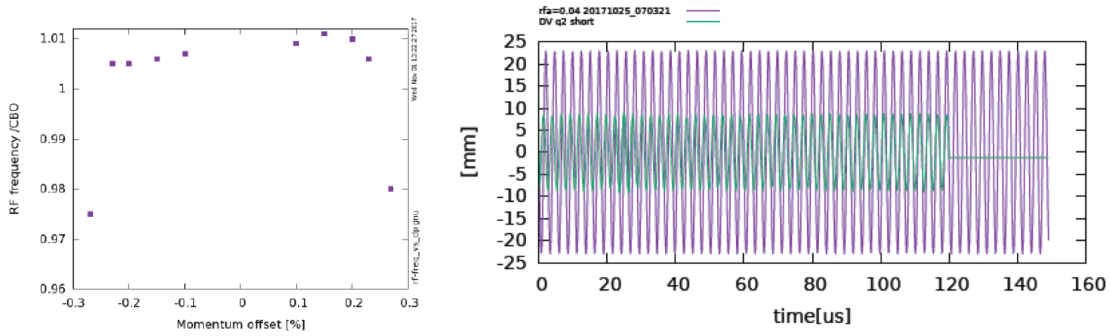

(a) (b)

FIG. 10: (a)Most effective RF frequency vs. muon momentum. Note that near the quadrupole plates the gradient is small and the focussing is weak. The $f_{RF} = 0.985$ for some damping at all momenta with a 20 μs RF pulse. (b) The RF has no effect on the on-momentum particles, i.e. the magic momentum particles.

But nothing is perfect. In the injected distribution there is a portion of the phase space, albeit a portion containing a small fraction of the total, for which the RF quad is distabilizing. The RF is effective as long as the off momenta muons all initially emerge from the very center of the inflector. But there is the occasional muon that will have finite displacement. Consider for example a muon with $\Delta p/p = 0.1\%$ just at the edge of the inflector aperture with 9 mm offset shown in Figure 11(a). The particle is driven to large amplitude by the RF field. Note that for this particular muon, the effective dispersion at the inflector exit is not zero, but $\eta = x/\delta = 9$m and that dispersion is increased by the RF quad.

We next study the effect of the RF quad field on a distribution with $\Delta p/p \sim 2\%$, and $\epsilon_x = \epsilon_y \sim 0$ and zero length. As usual the dispersio of the distribution is zero. The

h!

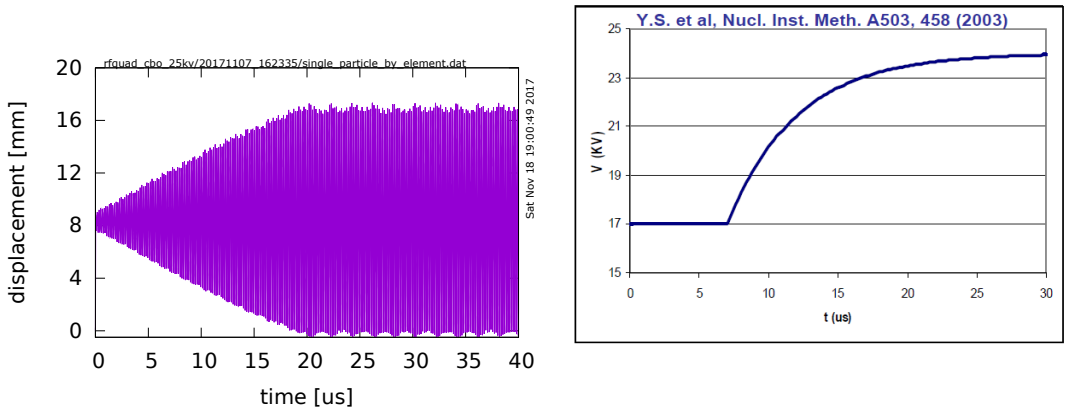

(a) (b)

FIG. 11:

distribution is inserted on the magic radius at the azimuth of the inflector exit. The muons are tracked for 300μs. Nominal quadrupole voltage is 25kV. The RF is applied to Q2 short with amplitude of 5kV for a duration of 20μs. There is no muon decay. The frequency is set to that which was earlier found to damp all momenta initially on the magic radius. We compute the evolution of the width of the distribution.

Insofar as the RF quad is an alternative to traditional E821 quad scraping, we also quantify its effectiveness in cleaning up the distribution by counting the number of muons that are lost after the RF pulse is turned off or the quads are ramped to their final voltage, that is in the window from 30 μs to 300 μs.

The quad parameters used in the simulation of E821 style scraping are given in Table II. The time dependence is as in Figure 11(b) (borrowed from the E821 quad NIM article). The following assumptions are made:

- Quadrupole final voltage is $\pm$25 kV
- Quadrupole scraping ramp is 18 $\rightarrow$ 25 kV
- The ramping time constant is 5μs.
- For the RF manipulation, the voltage on Q2 short is modulated at αf_{CBO}, where $\alpha \sim 1$, with an amplitude of 5 kV

Figure **??**(a) shows beam width (rms) as a function of time with traditional scraping and with the RF quad field. This is what we would measure at a single point in the ring as a function of time, the perfect fiber monitor for example. We see that at very early time the width is rather broad as the beam quickly fills the aperture. The distribution initially has zero length and zero emittance and as the high momentum muons fall behind and the low momentum move ahead, the momentum spread sampled at any given time is rather

Quad	Top	Bottom	Inner	Outer
Q1	+25	+18	25	25
Q2	+25	+18	-18	25
Q3	+25	+18	-18	25
Q4	+25	+18	25	-18

TABLE II: The E821 Scraping Parameters.

narrow and so is the beam width. At about 30μs the low momentum muons lap their high momentum counterparts and now the full momentum spread appears in a single time slice. This pattern repeats until the beam has completely decohered after $\sim 100\mu$s. The RF quad has very significantly reduced the width of the associated with a distribution of momenta.

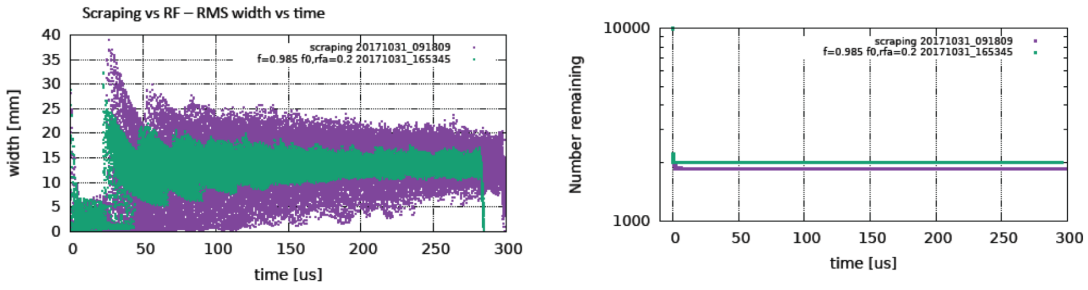

(a) (b)

FIG. 12: (a) Width vs time of a distribution that is initially gaussian with $\Delta p/p = 2\%$; emittance $\epsilon = 0$, zero length and zero angle and offset. The green is with RF quad, and purple with E821 scraping (b) Number of muons remaining in circulation vs time. Muons lost after beam manipulation (after 30μs) contribute to 'lost muon' systematic. Green is for muons with RF, and purple with E821 scraping.

The benefit of the RF quad is less striking for the somewhat more realistic distribution with finite emittance. Figure 13 shows the evolution of the beam width for a distribution with $\epsilon = 40$mm-mrad, $\Delta p/p = 2.0\%$, and zero length. The width of the distribution is slightly narrower with the RF quad. However, the number of muons remaining in circulation at the conclusion of the RF pulse is nearly 10% more than after the traditional scraping. The statistics are insufficient in this study to quantify the relative number of lost muons after the beam manipulation.

Finally the evolution of a distribution with $\Delta p/p = 2\%$, $\epsilon = 40$ mm-mrad and rms length $\tau = 120$ ns is shown in Figure 14. Again, the effect of the RF quad is to narrow the width and improve the efficiency with respect to E821 scraping.

Next explore the implications of RF modulation of the quads for numbers of lost muons and include the effects of the distortion of the phase space distribution in propagation through injection channel and between the kicker plates. We begin with a distribution of 1M muons with $\sigma_p/p = 2\%$, $\epsilon = 50$mm-mrad, and the 120ns 'W' temporal shape. Particles are tracked through the inflector, into the ring, and are kicked into the storage volume. Typically about 38,000 muons are stored. As before there is no muon decay. We compare the number of muons lost in the interval 30μs to 300μs for three different configurations

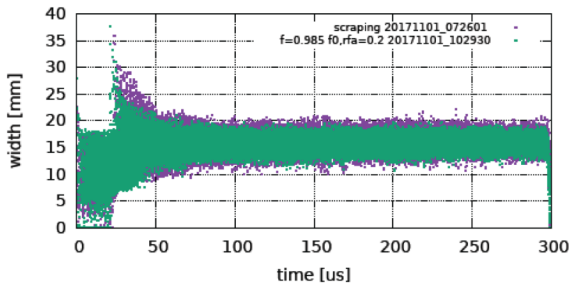

(a)

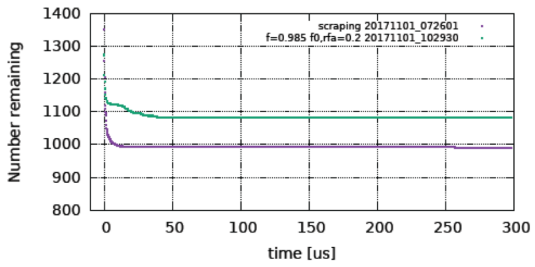

(b)

FIG. 13: (a) Width vs time of distribution that is intially gaussian with $\Delta p/p = 2\%$; emittance $\epsilon = 40$ mm-mrad, bunch length $\tau = 0$. The green band is with RF quad, purple with E821 scraping (b) Number of muons remaining in circulation vs time.

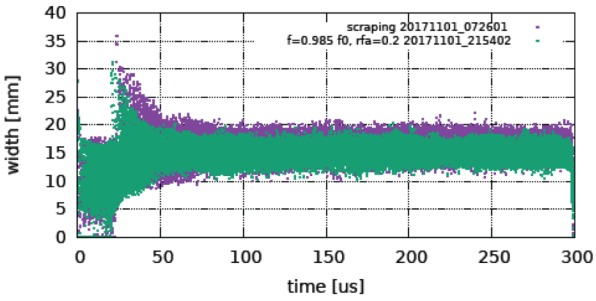

(a)

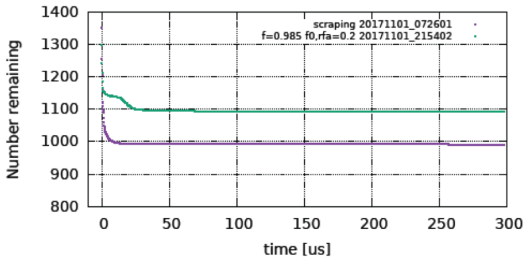

(b)

FIG. 14: Width vs time of distribution with $\Delta p/p = 2.0\%$, $\epsilon = 40$mm-mrad and $\tau = 120$ ns. The green band is with RF, purple with E821 scraping. (b) Number of muons in circulation vs time Green is with RF, purple with E821 scraping.

- No scraping of any kind.
- E821 style RF scraping as described above
- RF quadrupole 20μs pulse.

The number of muons vs time for the three configurations is shown in Figure 15 and summarized in Table III. Capture efficiency is somewhat greater with RF quad versus E821 scraping, but there are significantly fewer lost muons with E821 scraping.

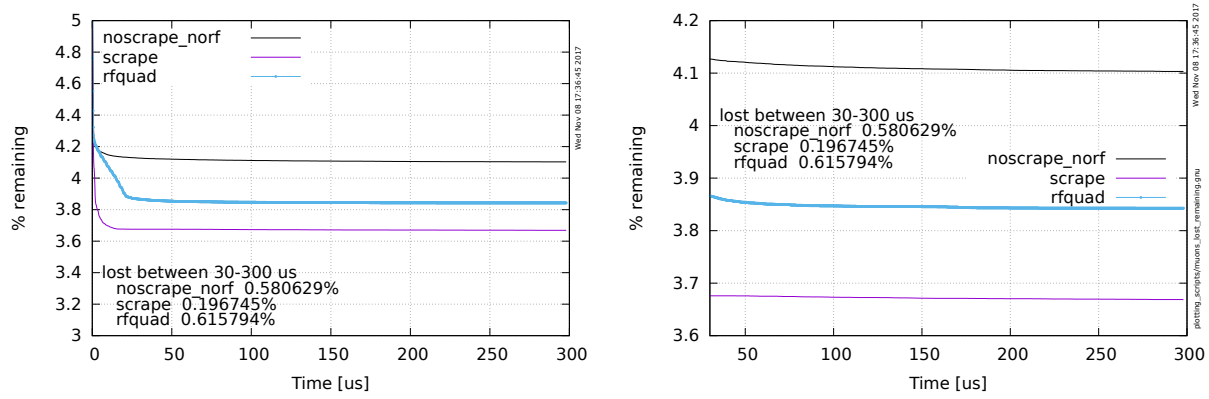

(a) (b)

FIG. 15: Distribution of muons ($\sigma_p/p = 0.02$, $\epsilon = 50$ mm-mrad, W-pulse shape) is propagated through the injection channel, inflector, and kicker gap. Temporal and spatial profile of the kicker field is based on maps and measurements, for each of the three configurations. The plots show the fraction of injected muons that are circulating as a function of time. Left and right are the same data with different vertical scale.

Configuration	Fraction of muons lost	Capture efficiency
No scraping or RF	0.581%	4.1%
E821 scraping	0.197%	3.68%
RF quad	0.616%	3.85%

TABLE III: Lost muon statistics.

III. DETAILS OF THE RF SYSTEM

A. The basic layout

The RF system is applied to the quadrupole system by capacitively coupling them to the quadrupole plates. The RF is added on top of the high voltage that produces the electrostatic quadrupole field. The quad system will need to be modified so it can be operated in the E821 scraping method, or with the RF. It will be modified so that the "input" for the RF is terminated when the RF is not connected as shown in Fig. 16. This option was studied to demonstrate that the current on the 1 MΩ resistor and other currents to see if there might be issues that are not there before the terminating resistor R2 is added.

A schematic of how the RF signal is sent to the quadrupole plates is shown in Fig. 17. The cartoon of how these signals are used on the quad plates is shown in Fig. 1 in the introduction.

A simulation of the current

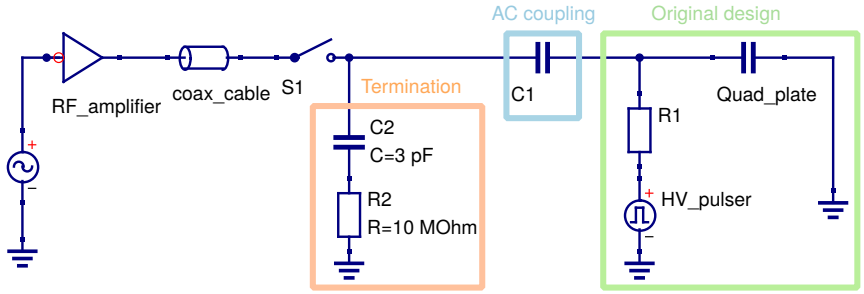

FIG. 16: The quadrupole circuit showing the addition of the RF system. The RF system isl capacitively coupled to the quadrupole plates through C1. When the RF system is not connected, the line to the plates is terminated through C2 and the 10 MΩ resistor R2.

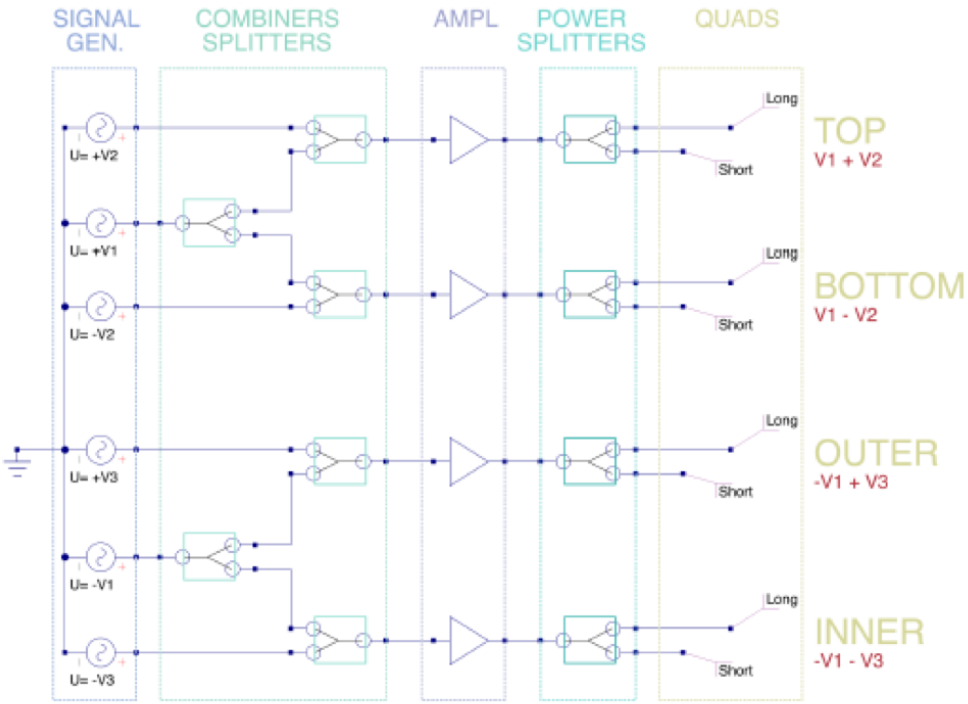

FIG. 17: The RF signal generators, splitters and the connections to the quadrupoles. This figure gives the details of the left-hand side of Fig. 16

B. RF Tests at Fermilab

The RF system prototype was tested at Fermilab in August 2017. It is documented in docdb note 4301 by Young-Im Kim. A schematic of the setup is shown in Fig. 18

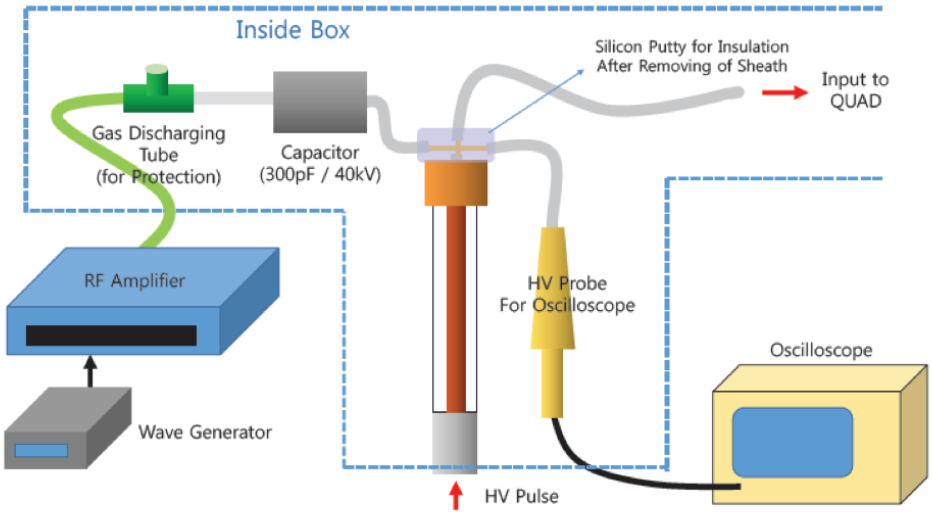

FIG. 18: A schematic of the experimental setup used to test if the RF system would be compatable with the existing pulser system.

IV. DISCUSSION AND CONCLUSIONS

V. REFERENCES

[1] G. Bennett, et al., (Muon $(g-2)$ Collaboration), Phys. Rev. **D73**, 072003 (2006).

[2] Y. Orlov and Y. Semertzidis, E821 Note #431, (2003).

[3] Seungcheon Kim, GM2-doc-7607-v1, 28 Jul 2017. See also Diktys Stratakis, GM2-doc-4461-v1, 18 Oct 2016, and Seungcheon Kim GM2-doc-4886-v2, 03 Feb 2017.

RF Amplifier Data Sheet

TOMCO

BT-AlphaA Series
10kHz-3MHz
250W, 500W

- NMR, MRI, EPR
- Radar
- Ultrasonics
- Test & Measurement



The BT-AlphaA series is a range of class AB RF power amplifiers covering the 10kHz to 3MHz frequency range.

- Rugged, solid-state design - high reliability
- Extremely high phase and amplitude stability
- Very fast pulse rise/fall times
- High linearity
- Very low interpulse noise
- Competitively priced

Suitable for NMR, MRI, NQR, EPR, pulsed radar, ultrasonics and other scientific applications.

www.tomcorf.com

BT-AlphaA Series	
Model numbers	BT00250-AlphaA / BT00500-AlphaA
Rated power	250W / 500W minimum[1]
P1dB	200W / 400W minimum[2]
Gain	54dB / **57dB** minimum
Type	Class AB MOSFET
Frequency	10kHz-3MHz[3]
Gain flatness	±1.5dB maximum (measured at 1/10th rated output power)
Max. duty cycle	20%[4]
Max. pulse width	100ms[5]
Rated power in CW mode	25W / 50W[6]
Pulse droop	0.5dB maximum across 100ms pulse[7]
Pulse rise and fall times	100ns typical using a pre-gate RF input signal
Gate delay	Rising edge: 2µs typical Falling edge: 1µs typical[8]
Harmonics	Odd: -20dBc typical, -12dBc maximum Even:-30dBc typical, -20dBc maximum
Spurious	<-70dBc maximum
Output noise (blanked)	<10dB above thermal (100kHz bandwidth)
Phase change/power	<5˚ from -40dB to full power
Phase stability	<1˚ across 100ms pulse
Output sample	-50dB into 50 Ω (forward voltage sample)
Input/output impedance	50 Ω nominal[8]
Load VSWR	Tolerates at least 3:1 @ full rated power without shut down[9]
Remote interface	Parallel status monitoring via 25 pin D connector[10]
Connectors	RF output: N type RF input, gate, sample:BNC[11]
Cooling	Forced air
Indicators	DC Power, RF Power, Enable, Selected, Mismatch, Over-temp, Over-duty, Shutdown
Protection	Load VSWR, duty-cycle, pulse width, over-temperature
Gain control range	10dB minimum for 0-5V control voltage
RF drive RF gate (blanking)	0dBm nominal, 10dBm for no damage 0-5V CMOS
Physical	19" Wx 500mmD x 180mmH (3RU x 19" rack mounting), 13kg / 17kg
Mains power	110-240V, 50-60Hz, single phase, 1kVA / 2kVA max.[12]
Compliance	CE

1. PEP for input power of 1mW
2. Minimum output power at 1dB gain compression
3. The amp provides useful power outside this range, but performance is not guaranteed
4. Duty cycle is internally limited in pulsed mode
5. Maximum gate pulse width in pulsed mode (internally limited)
6. CW mode automatically enabled at output power level less than approx.10% of full rated power
7. Measured at max. pulse width at nominal P1dB level
8. Rising edge measured from rising edge of GATE pulse to 90% RF output voltage.
   Falling edge measured from falling edge of GATE pulse to 10% RF output voltage
9. Self resetting protection shuts the amplifier off if the load SWR is excessive
10. Pin out at www.tomcorf.com/pdf/interface.pdf
11. Other connector types available on request
12. 3-pin IEC. mains supply must include an earth

FIG. 19:

BT-AlphaA Series
10kHz-3MHz
250W/500W

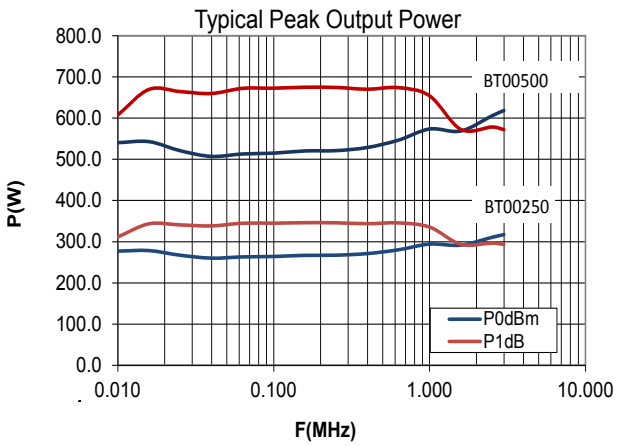

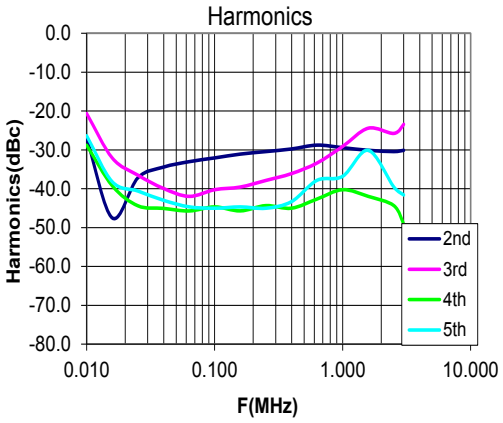

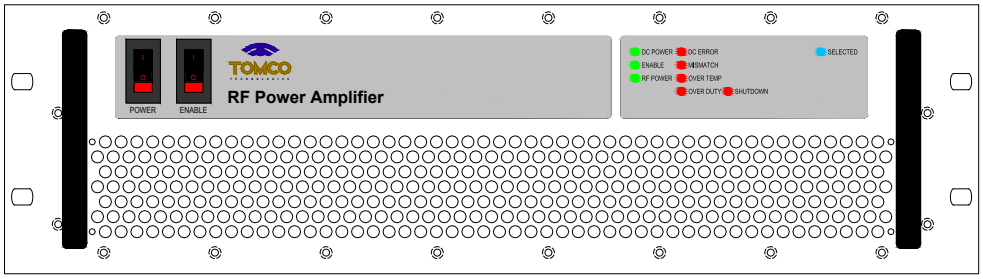

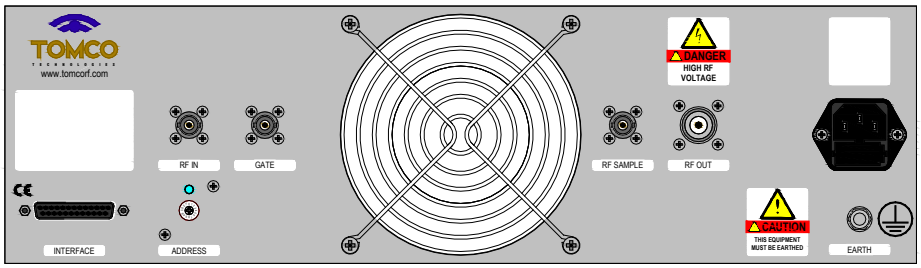

Tomco Technologies
38 Payneham Rd, Stepney
South Australia 5069
www.tomcorf.com

Tel: +61 8 8362 2902
Fax: +61 8 8362 2912
Account enquires: accounts@tomcorf.com
Sales enquiries: sales@tomcorf.com

USA: +1 202 657 6844
UK: +44 20 3239 6847
Hong Kong: +852 8121 4277

FIG. 20: